Compression and shear strengths of sandy limestone and the role of the porosity: a case study

Yousr Koobaa[1,#] iD , Houda Guiras[1] iD , Mehrez Jamei[1,2] iD

Case Study

Abstract

This paper focuses on the study of the mechanical behavior of sandy limestone rocks. These rocks are provided from the historical caves of El Haouaria, which are located on of the North Eastern seacoast of Tunisia, and were created during the Punic era. Nowadays, these caves suffer from cracks, randomly distributed with a variable opening size. While, it appears that damage risk monitoring of the El Haouaria caves is a priority, linked questions concerning the mechanical behavior of the cave's rocks still remain, mainly because of its variable porosity and evolution with time. Understating its behavior will be a main tool to build a monitoring program, leading to an optimum reinforcement solution. Aside from uniaxial tests performed on several undistributed samples of a porosity ranged between 30 % and 50 %, triaxial tests were also conducted on undistributed specimens with a porosity of 30 % and 50 %. All the results showed a significant effect of the porosity on the mechanical properties. The nonlinear Hoek-Brown criterion was used to model the shear failure, introducing few changes in order to consider the porosity influence. It was found that this criterion provides a satisfactory estimation of shear strength and its dependency on the porosity. Intact rock parameters and their porosity dependency were determined from compression and bending tests of undistributed samples. However, in situ rocks were considered as micro-fissured, principally for U3 layer, and the Geological Strength Index (*GSI*) was determined for the fissured rock.

1. Introduction

The caves of El Haouaria are carved inside sedimentary rock mass dating from the Punic era. They are a historical monument located in the seacoast of the Cap Bon region in the North East of Tunisia (Figure 1). The caves have undergone the impact of climate change, such as humidity cycles characterized by a high variation of the relative humidity across the day. Evidently, the caves have been exposed to a range of seasonal temperature variation, atmospheric evaporation and humidity cycles. The caves are composed of 5 types of rocks, successively noted U1, U2, U3, U4, U5, respectively from base up to ground surface (Figure 2). The rocks composing the caves are biogenic sedimentary rocks, which are induced by cementation and compaction during sediment digenesis. Porosity varies from 25 % to 55 %. Currently, the caves contain a crack network that compromises their stability. Due to potential risk of collapse of cave parts, three caves among the set were completely closed off tourist visitors (Figure 2). In order to preserve these caves and predict the risks of failure, the Tunisian National Agency for the Protection of National Monuments, has proposed a research study, starting by the investigation of the behavior of the rocks.

All the reasons cited above highlight the importance of the investigations on the origins of the cracks. The authors proposed a two-phase study. The first was to understand and define the caves of El Haouaria rock's mechanical behavior. Then, the last stage of the study, which is not included in this paper, will be the reinforcement of the three caves based mainly on the conclusions and the failure model retained in this paper.

Laboratory tests have been performed on undistributed samples provided from blocks placed near the caves, since sampling from the caves was not permitted. This paper focuses particularly on compressive and shear behavior of these rocks in their current state. The dependency of compression strength and shear strength was quantified.

Regarding research literature, many studies have focused on the sustainability of rocks involved in restoration of monuments (Yu & Oguchi, 2010; Al-Omari et al., 2015, Aldoasri et al., 2017, Rahmouni et al., 2017). Several previous studies have described mechanical compaction in various porous rocks (Baud et al., 2004) and carbonate rocks (Evans et al., 1990, Nicolas et al., 2016). Some researchers at universities and at industries were carried out specifically on soft rocks. Kanji (2014), for example, discuss the critical issues in soft rocks. In fact, the author discussed the currently widespread classification systems of weak and soft rocks. As a conclusion of the cited paper, it was established that besides uniaxial compression strength (*UCS*), often admitted as criterion to classify soft rocks (for example the upper limit of 25 MPa was practically retained), porosity of rocks was also considered as a parameter. Thus, Bosio & Kanji (1998) proposed a correlation between porosity, absorption (%) and *UCS*. Other researchers have investigated the mechanical behavior of soft rocks with high porosity and low mechanical strength (Guilloux, 2005; Asef & Farrokhrouz, 2010). Whereas some researchers, such Elliott & Brown (1985), considered that high porosity determines rock's belonging to soft rock class. Relying on these results, many authors have significantly contributed to a general understanding of strength and elastic deformation of soft rocks (e.g. Price & Farmer, 1979; Daoud et al., 2017; Baud et al., 2014).

In the current study, the authors tested rocks exhibiting a variable mineralogy and a wide range of porosity. The authors also focused on the shear behavior of such sandy limestone rock and the effect of porosity on the maximum deviatoric stress and then on shear strength. Water content during shear tests was considered constant since suction was controlled. Triaxial tests show that stress-strain response changes from fragile behavior to ductile behavior.

On the other hand, the generalized Hoek-Brown model was applied to predict compressive and shear strength. The role of porosity was indirectly taken into-account when main parameter m_i was introduced as function of both compression and tensile strengths (Hoek & Brown, 2019).

The discussion in this paper focuses on the efficiency and relevance of generalized Hoek-Brown criterion for U3 rock modeling of El Haouaria caves. The model was used to predict the behaviour of the samples with variable porosity and then the behavior of soft intact rocks constituting the cave's structure in which the fissures are randomly distributed, with variable length and opening; for which the authors used *GSI* system as it was recently discussed in the paper of Hoek & Brown (2019).

2. Materials and methods

The caves are carved inside the consolidated dunes (aeolianites), formed during the Late Quaternary period (Tyrrhenian stage). These dunes are composed of a stratification of five geological layers (Paskoff & Sanlaville, 1983). The base layer U1 is composed of limestone debris and quartz and have oblique stratifications. The second layer U2 is composed of limestone debris and quartz without stratification. The third layer U3 is very thick. It is made of limestone debris from fossils (algae, echinoderms, mollusks), rare foraminifera, quartz grains (scattered, or in clusters and have a small size). The fourth layer U4 is composed of limestone debris and quartz without color with variable thickness (from 30 cm to 1 m) and has frequent foraminifera and pellets (totally micritic grains). The upper layer is thin and topped with a crust composed of limestone debris from fossils algae, echinoderms, mollusks and quartz grains. These caves provided the rock material that was once used for building Carthage, as shown in Figure 1.

The caves are large semi-dark caves made of latomies, carved in the shape of a pyramid with a narrow upper opening. There is also some narrow opening that communicate between caves. Due to bombing raids during the Second World War, followed by natural collapses, wider lateral openings were created. Visits to the site became possible (Harrazi, 1995).

The authors focused on the study of mechanical properties, in particular U3 (the third layer) rock properties, since it is the thickest and contains a series of developed cracks that compromise cave stability (Figure 2b). Therefore, unconfined compression tests and triaxial tests were performed on samples extracted from this same layer, but with various initial porosities. Micro-structural characteristics and mineralogical composition of U3 rocks were examined by light microscope, scanning electron microscope (SEM), XRD analysis and chemical analysis (for more details, see Koubaa et al., 2018). Chemical analysis and diffraction technique (XRD) showed that the minerals of U3 rocks are composed mainly of calcite ($CaCO_3$, SiO_2) and some other minerals such as Aragonite, halite (Koubaa et al., 2018) The. U3 rocks were examined by light microscope and scanning electron microscope (*SEM*). It has been shown that the rocks are grainstone, well graded and very porous. They were composed of algae debris (*Al*), lamellibranches, gastropods echinoderms (*Ech*) and Quartz grains (*Qz*). For this mineralogical composition, experiments show that rocks had various porosity and different particle size distribution trends. Rock porosity varied from 25 % to 55 %. Besides, the cement connecting the grain is very thin which reinforce its classification as a soft rock. Previously, it has been shown that environmental cycles cause increase of porosity by dissolving some minerals in the rock (Koubaa et al., 2018). The *SEM* analysis showed that the cement is thin, opaque (thickness close to 35 μm) and covers the majority of grains (Figure 3). Pores between grains are interconnected. The digenesis of the cement is precocious; except when salt dissolves under the effect of water, then deposits of salt and minerals between grains are created.
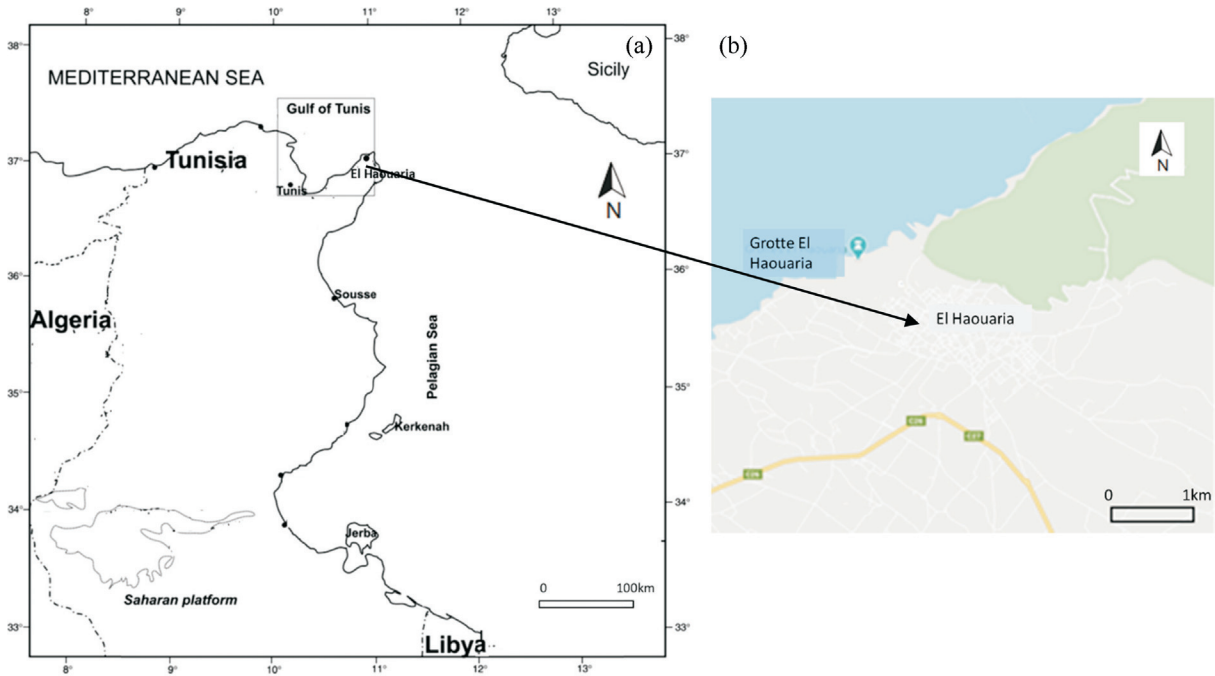
Figure 1. (a) El Haouaria location in Tunisia (b) El Haouaria caves location.
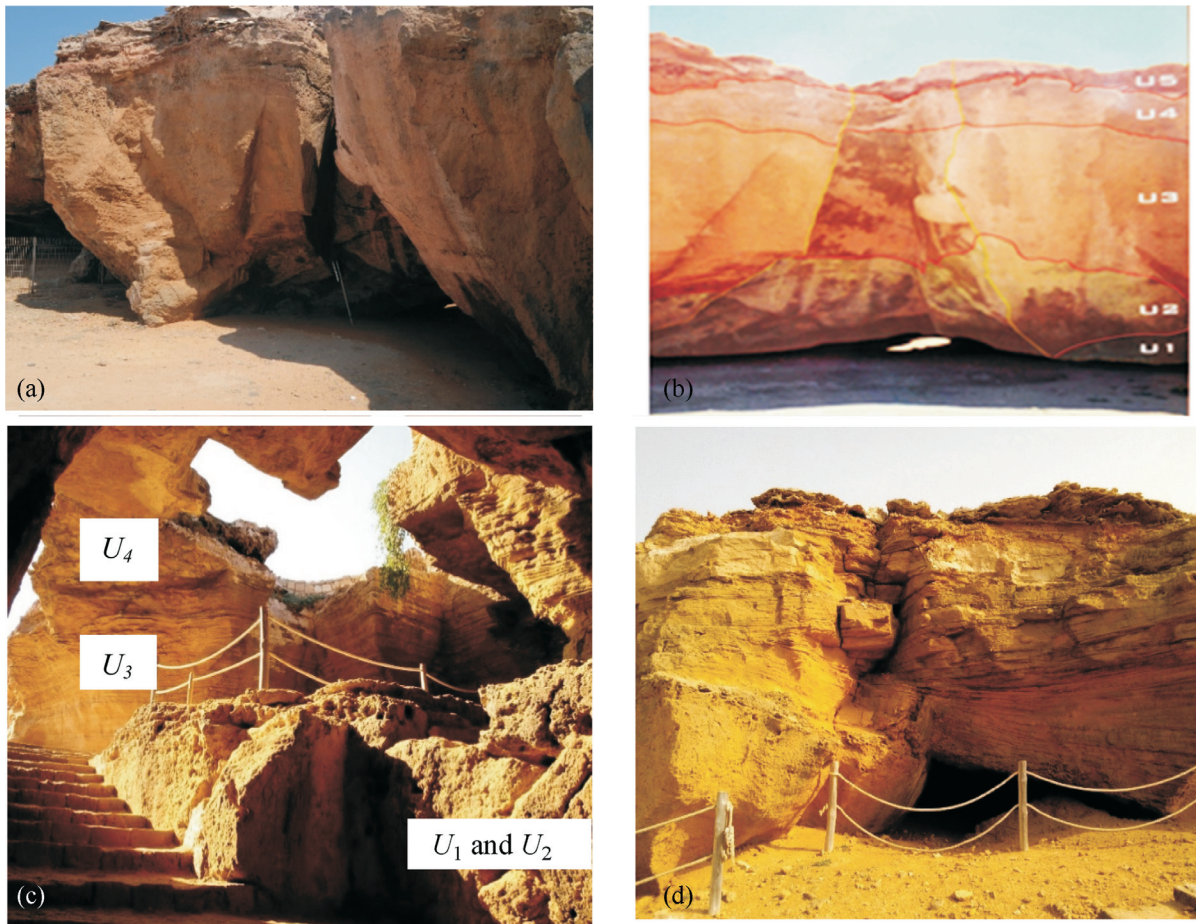
Figure 2. Photographs of caves: a) front of caves, b) Stratified layers called U1 to U5 that constitute the caves, c) the surface of well-distributed caves, d) layers of fractured caves.
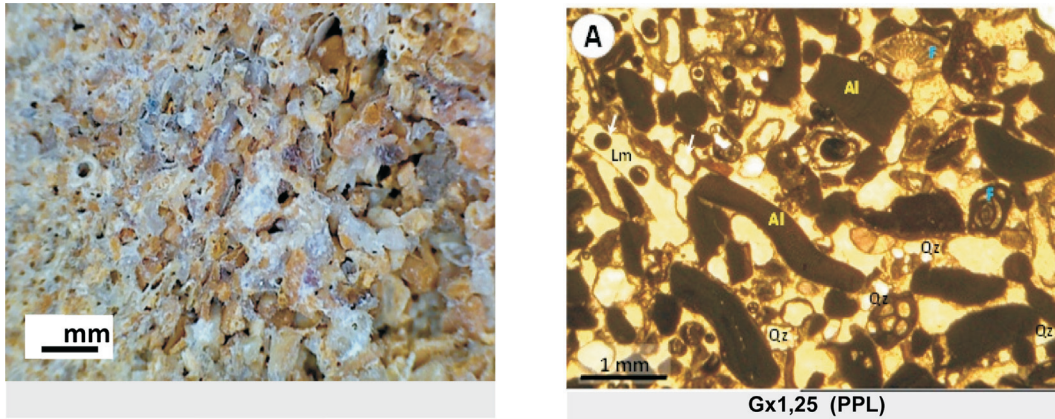
Figure 3. Thin sections (1 mm and 200 μm) of specimens from U3 layers in plane polarized light U3 (*AL*: algae, *QZ*: quartz, *Ech*: echinoderms, *F*: Foraminifera, *Lm*: Lamellibranch).

This leads to replacement of pore connectivity (Figures 4-a, 4-b).

First porosity was measured for each tested sample. Tests were repeated minimum three times. An average value was retained. Porosity was determined according the ISO 5017 Standard (ISO, 2013), which defines porosity as the ratio of total pore volume in a porous body to its apparent volume (total volume). So, porosity (n) was computed as following:

$$n = 100 \frac{V_{void}}{V_{total}} = 100 \frac{V_{total} - V_{solid}}{V_{total}} = 100 \left(1 - \frac{\rho_a}{\rho_s} \right) \quad (1)$$

where V_{void} is the volume of voids, V_{solid} is the volume of solid and V_{total} is the total volume.

The authors have used a simplified method to determine apparent density by measuring the dimensions of specimens to obtain the total volume, and the mass of solid. Apparent density is computed as:

$$\rho_a = \frac{M_s}{V_{total}} \quad (2)$$

and specific density is computed as:

$$\rho_s = \frac{M_s}{V_s} \quad (3)$$

where specific density ρ_s was determined according to the standard NF P94-054 (AFNOR, 1991), using a Pycnometer with a volume of 50 cm³, which resulted in 2.72 g/cm³. Three values of mass were determined as following:

- The mass of the Pycnometer filled with water to obtain the mass M_w,
- The mass of the dry mass of the sample of crushed rock (very fine) to obtain: M_1
- The mass of the Pycnometer filled with dry rock, very fine, and filled with water: M_2

The density of solids was thus determined as follows:

$$\rho_s = \frac{m_s}{m_e} = \frac{M_1}{M_w + M_1 - M_2} \quad (4)$$
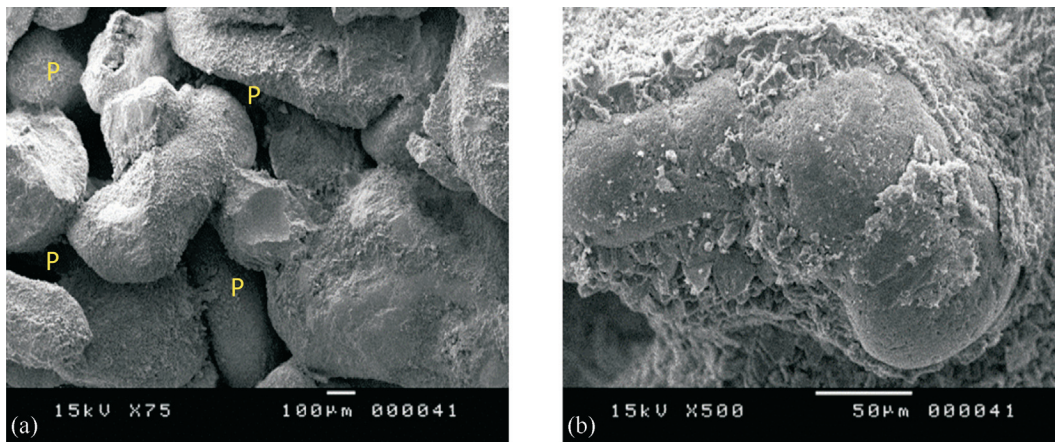
Figure 4. *SEM* micrographs of rock from El Haouaria caves U3: a) grains and bonding material and inter-granular porosity, b) lodges of a foraminifer partially covered by a fine cement 10 to 20 μm thick.

Two types of compression tests were performed on U3 specimens. In fact, separately compression force -controlled (using Instron 4485 press) and displacement-controlled rates were performed on rectangular prism specimens (of square section with edges of 4 cm, and a height of 8 cm). Due to low strength and randomly distributed porosity, specimen preparation for testing were problematic. Diamond discs using water were specifically used to obtain specimens from blocks from the caves field. Uniaxial compression device has a maximum load capacity of 300 kN. Force was controlled with a 1/100 of standard deviation value. A number of 23 dry specimens of uniaxial compression tests were tested. The porosity of each sample was computed using sample's solid density, mass and volume values. Sample's porosity varied from 25 % to 55 %.

In the other hand, series of uniaxial compression tests, under controlled displacement rate (4 mm/min), were added. However, for these series, specimens were cylindrical of a 10 cm diameter and a 20 cm height (Standards AFNOR P94-420, 2000, and ASTM D 7012-04, 2004). The force-controlled tests were performed on sets of 5 pieces of U3 and samples with porosity ranging between 30 % and 50 %.

From stress-strain curves, mechanical characteristics, such as uniaxial compressive strength σ_c, Young's modulus E and Poisson's ratio ν were identified. Meanwhile, some specific tests as ultrasonic tests were performed in order to measure the dynamic elastic modulus and its dependency on porosity. Wave's velocity (V_p) was recorded according to AFNOR P94-411 (AFNOR, 2002) Standard, on cylindrical specimens of 40 mm diameter and 80 mm height. The specimen was placed between a transmitter of ultrasonic wave (with frequency of 54 kHz) and a receptor.

The ratio of the distance separating the transmitter from the receptor to the time taken by a wave (P) to cross it gives the velocity V_p. The time was measured using PUNDIT ultrasound machine.

Adding two series of uniaxial compression tests, some indirect tensile tests were performed using bending beam tests. These tests aim was to obtain tensile strength.

In addition to the demonstrate the role of the porosity in the uniaxial compression tests, the authors have to emphasize that our original contribution is the report of results of triaxial tests, which have been performed on specimens with conventional dimensions (a diameter of 38 mm, and a 76 mm high) with porosity variation.

It is also important to mention here that triaxial tests were carried out only on sets of specimens with average porosity of 30 % and 50 %. The limiting factor was the difficulty in sampling from the same blocks due to the constraint of keeping the same physical properties of specimens. The triaxial device had automatically controlled stresses. Axial (ε_1) and radial (ε_3) strains were obtained using axial and lateral transducers. For samples with 50 % porosity, the confining pressures were respectively, 500 kPa, 800 kPa and 1200 kPa. However, due to limitation of load frame (allowable axial force), confining pressures for specimens of 30 % porosity were 100 kPa and 500 kPa.

The radial deformation ε_3 response was monitored with an electro-optical laser system mounted on two diametrically-opposite sides. Vertical displacements were measured by the means of an external *LVDT* (including corrections due to cell deformability). The triaxial setup comprised two electro-pneumatic pressure regulators (*QB*1 Proportion Air) for chamber and axial piston pressure.

Two stepper motors using air pressure regulators were used to continuously control both deviator and confining stresses. Stepper motors and measurements of 14 sensors were managed by automatic data acquisition and control system that allow to apply a generated stress and to perform strain-controlled tests (for more details see Romero, 1999).

3. Experimental results

3.1 Physical properties

The physical properties of the rock samples are given in Table 1. Low dry unit weight for high porosity were obtained. Therefore, a large dry density variation corresponds to the porosity range.

3.2 Elastic properties

Figures 5a and 5b respectively show the dynamic elastic modulus (from Ultrasonic tests and using Equation 5) and the static elastic modulus (defined as the initial secant tangent between unconfined compression stress and corresponding strain). The two elastic moduli were obtained from several tested specimens with different porosities. Both curves indicate the same trend of dynamic and static moduli with porosity. Indeed, when porosity increases, elastic modulus decreases significantly.

However, it has to be emphasized that due to the difficulty to reproduce the same porosity for prepared undistributed specimens (remember that such specimens were extracted and prepared from a given large block), it was very problematic to prepare specimens with a longed for porosity for both unconfined compression tests and ultrasonic tests. For this reason, curves presented in the following, for Ultrasonic tests and static compression, tests corresponded to different ranges of porosity.

Dynamic elastic modulus was computed as given in Equation 5:

Table 1. Physical properties of tested rocks.

Physical characteristics	Rock U3
Dry density (g/cm^3)	from 1.5 to 2.5
Bulk density (g/cm^3)	2.72
Porosity	from 25 % to 55 %
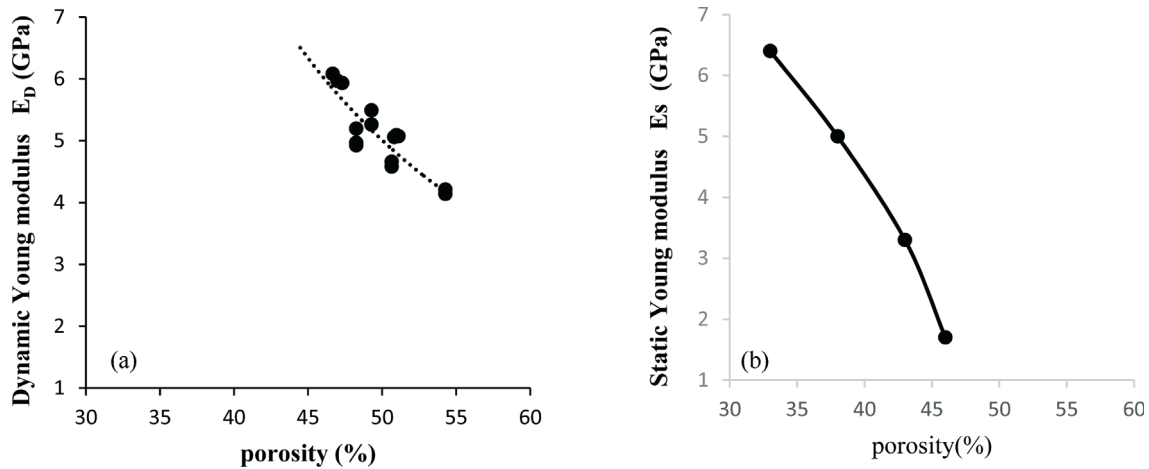
Figure 5. Elastic moduli vs. rock porosity: a) dynamic moduli, b) static moduli.

$$E_D = \rho(V_p)^2 \frac{(1+\nu)(1-2\nu)}{(1-\nu)} \quad (5)$$

where ρ is the rock density by Equation 2, ν is the Poisson's ratio which is supposed equal to 0.33, Vp is the velocity of the primary (compression) wave (in m/s).

3.3 Effect of porosity on uniaxial compressive strength (*UCS*)

Because U3 layer is fissured, all experiences were prepared using blocks provided from this layer. It was found that *UCS* decreases from 14 MPa to 1.2 MPa since the porosity increases from 30 % to 50 % (Figure 6). These low *UCS* values correspond to soft rock characteristics. The *UCS* was controlled by porosity (see for instance Koubaa et al., 2018). To reach compressive failure, stress-strain curves exhibited two important features. The first is that axial strain at failure increases with porosity (it varies from 2 %

to 4 %, when porosity varies from 33 % to 46 %). The second fact is that post-failure behavior has a significant negative hardening.

In addition to the experiments performed specially to provide a database for the modeling, the authors performed bending tests. The results of indirect tensile strength (*ITS = Rt*) indicated that the *ITS* varies from 0.3*UCS* to *UCS*. The *ITS* is approximately equals to the *UCS* for the high porosity of 50 %.

3.4 Triaxial compression results

Deviatory stress-strain-curves were obtained at different confining stresses increasing from 0.5 MPa up to 1.2 MPa. Deviatory stress q is defined as $q = \sigma_1 - \sigma_3$. Stresses σ_1 and σ_3 represent respectively axial and lateral stresses. In this paper, the authors assume that compressive stresses and contraction strains are positive.
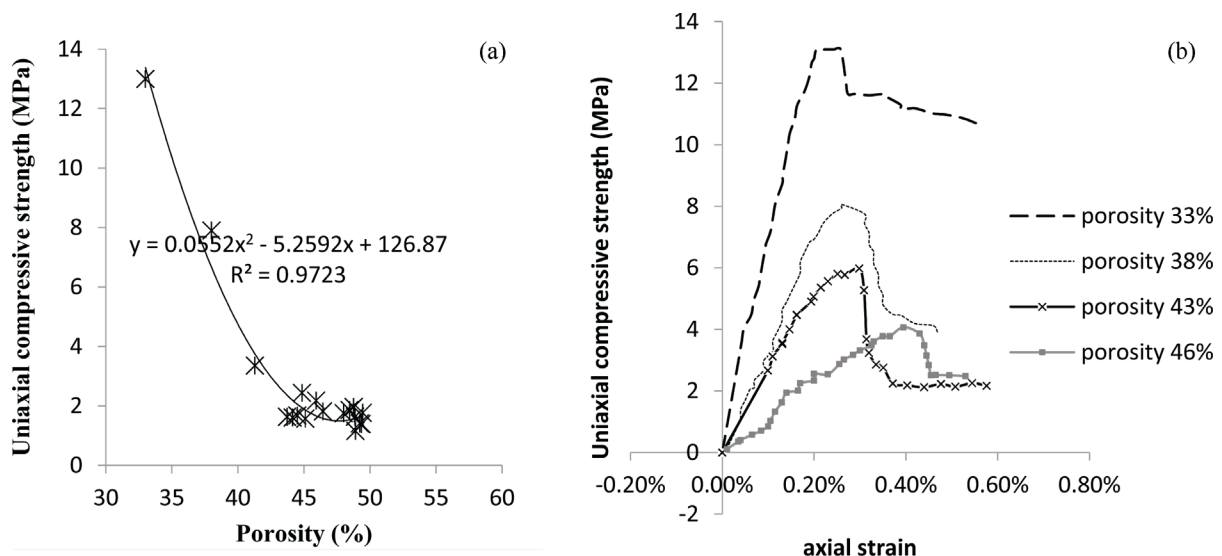
Figure 6. Uniaxial compressive strength vs. : a) porosity, b) axial strain.

Test results are illustrated in Figures 7 and 8 in terms of deviatory stress ($q = \sigma_1 - \sigma_3$) vs. strain (two kinds of strain were measured: axial strain ε_1, and radial strain ε_3). Volumetric strain $\varepsilon_v = \varepsilon_1 + 2\varepsilon_3$ was then deduced. Each curve in Figures 7 and 8 was identified by its corresponding strain.

As it will be discussed below, two series of specimens were tested with different average porosity ranging of 30 % to 50 %. In addition, for a confining stress of 0.8 MPa, two kinds of rock specimens were tested (provided from two blocks from U3). Figures 7a to 7d provide results associated to a porosity of 50 %. Figures 8a to 8b provide results corresponding to porosity of 30 %.

Two main conclusions can be drawn from the trends indicated in Figures 7 and 8:

(1) In Figures 7a and 7b, the curves are characterized by a linear elastic deformation of axial strain of 2 % and 4 %, respectively. Maximum deviatory stress was observed around 2.5 MPa and 3.5 MPa, respectively associated to 2 % and 4 % axial strain for σ_3 = 800 kPa and σ_3 = 500 kPa, respectively. Moreover, as shown in Figure 7, the deviatory strain tendency displays an asymptotic behavior (two phases: elastic and perfectly plastic for relatively lower confinement stresses), and a hardening behavior for higher confining stress.
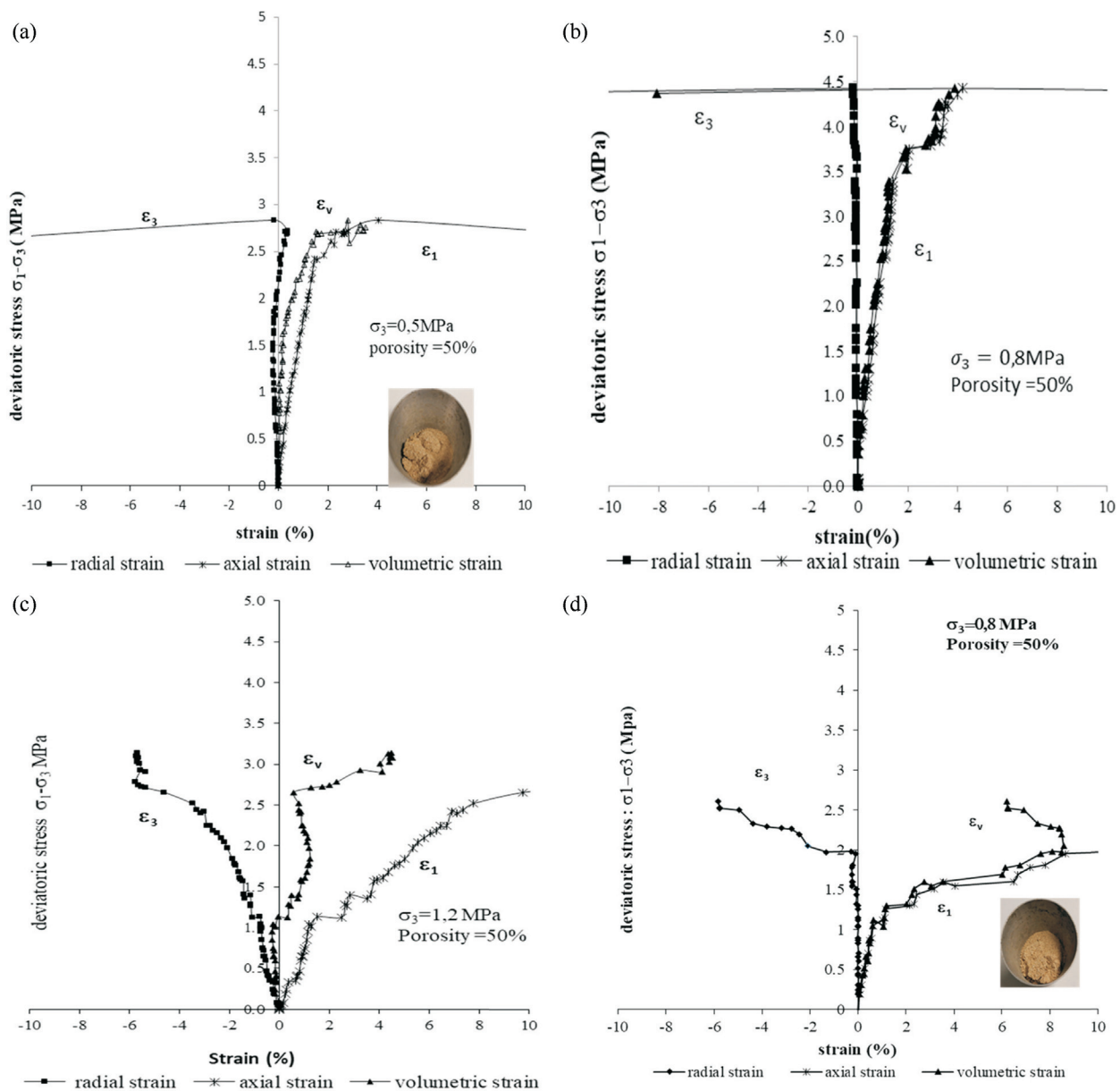
Figure 7. Deviatory stress vs. strains (axial, volumetric and deviatoric strains) under confining stress for values of a) 0.5 MPa, b) 0.8 MPa, c) 1.2 MPa, d) 0.8 MPa.

(2) In Figures 7c and 7d, respectively, the curves exhibit a typical behavior of compact cataclysmic flow regime, where both samples display similar differential stress-axial strain curves. Indeed, both samples display strain hardening, large strains and no stress drop. Beyond these stress levels, deviatory stress provided a significant contribution to the compact strain, and no shearing is observed.

According to visual observations on the tested specimens, no shearing localization was observed. As the number of cracks created in samples progressively rose during deformation, tendency of brutal crushing of samples under triaxial stresses was frequently observed for low confining stress.

All these features are commonly attributed to cataclysmic (or ductile) flow regime. As confining stress increases, inner structure of sandy limestone becomes more compact and hence and fracturing becomes inhibited. Deformation changes progressively from ductile to hardening behavior (see Figures 7a and 7b and then Figures 7c and 7d). Since high confining stress suppresses initiation, growth and propagation of cracks, compaction phase before onset of dilatation lasts longer while fracture percolation occurs later on at high lateral stresses. From a volumetric strain evolution, dilatation appears after some contractive volume values. Dilatation appears much later (for higher axial strain) with an increasing lateral confining stress.

On the other hand, results corresponding to 30 % porosity clearly showed an elastic response followed by some hardening (Figure 8a and 8b). A completely dilatory response was observed even for a relatively low confining stress. Naturally, compact rock exhibits a similar behavior as it was usually observed in the geotechnical field for dense sands. Initial high density did not allow a contractive movement of grains. Because of limited loading by the triaxial device, only two confining high pressures were selected, for which high values of deviator stress were reached.

4. Modeling of the experimental results

First, for intact rock mass, Hoek-Brown criterion was written as following:

$$\sigma_1 = \sigma_3 + \sigma_{ci}\sqrt{m_{br}\frac{\sigma_3}{\sigma_{ci}}+1} \qquad (6a)$$

Zuo et al. (2008, 2015) replaced m_{br} par the term; $\frac{\mu}{k}\frac{\sigma_{Ci}}{|\sigma_t|}$, where, $\mu = \tan\phi$ (ϕ is the crack surface friction) and $k = \sqrt{\frac{2}{3}}$. For $\phi = 45°$, $\mu = \tan\phi = 1$. The Equation 6a is then written as:

$$\sigma_1 = \sigma_3 + \sigma_{ci}\sqrt{\left(\frac{\mu}{k}\frac{\sigma_{ci}}{|\sigma_t|}\right)\frac{\sigma_3}{\sigma_{ci}}+1} \qquad (6b)$$

where σ_1 is the major principal stress and σ_3 is the minor principal stress, σ_{ci} is the compressive strength of intact rocks. In this equation, σ_t is the direct tensile strength. Table 2 summarizes the values for these parameters.

It is to be noted that, since tested specimens were considered undistributed, the authors admitted, the Hoek-
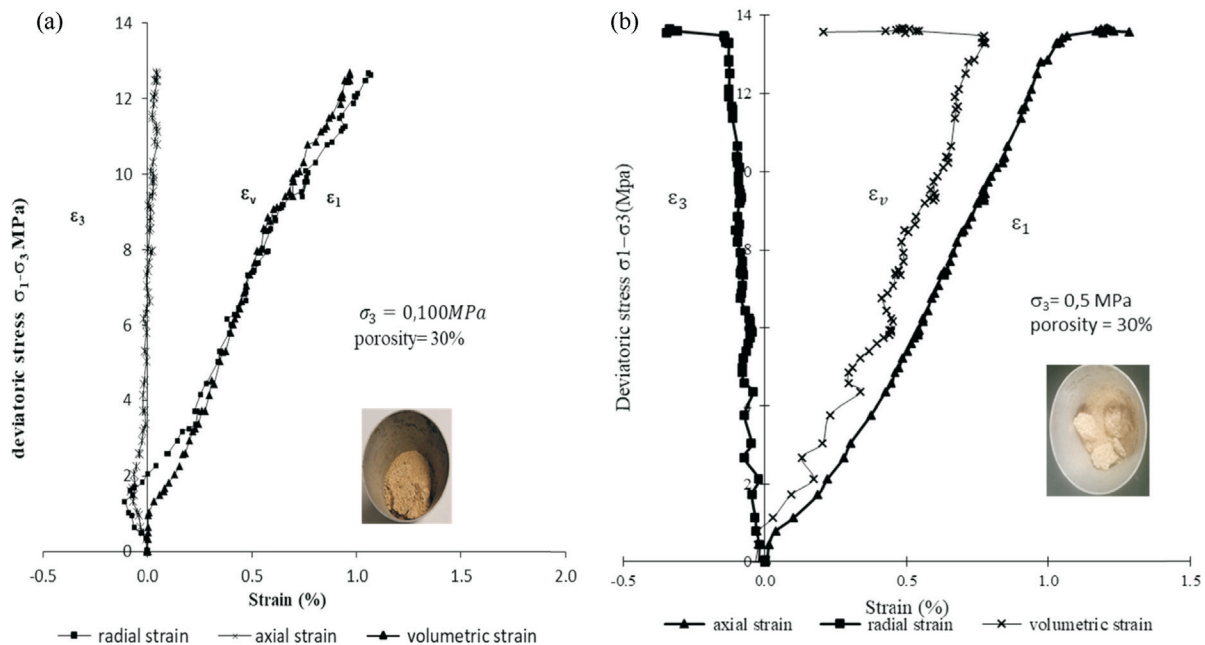
Figure 8. Deviatory stress vs. strains (axial, volumetric and deviatoric strains) for dry rocks under confining stress a) 0.1 MPa, b) 0.5 MPa. Rock samples were dried with a porosity of 30 %.

Table 2. Parameters of Hoek-Brown criterion, obtained by adjusting the experimental data.

Porosity	k	$\mu = \tan\phi$	Tensile strength ITS (MPa)	Correction to obtain an approximation value of direct tensile strength $\sigma_t = 0.7$ ITS (MPa)	σ_{ci} (MPa)	$m_{br} = \mu*\sigma_{ci}/(k*\sigma_t)$
30 %	0.82	1	2	1.4	10	10
50 %	0.82	1	0.6	0.7	1.7	5

Brown criterion given by Equation 6. Figure 9 shows the results of predicted compression and shear strengths. The tension cutoff was also included by the value of direct tensile strength obtained by a given correction of the indirect tensile strength ITS. The authors introduced a correction coefficient of 0.7 on the ITS measured by the three bending tests to obtain an estimation of direct tensile strength σ_t.

As it can be observed in Figure 9, experimental results were fitted based on Equation 6 and using the set of experimental results.

In the other hand, for fissured rocks mainly in U3 layer (see Figure 10), the authors propose here an extension of Hoek-Brown criterion (Generalized Hoek-Brown criterion, see Hoek and Brown, 2018). This is aiming to provide a failure criterion adjusted to U3 rock (typically a sandy limestone), which will be used for monitoring and eventually for a reinforcement solution proposal of U3 layer. Note that the degradation observed in U3 was taken into account via the parameters s, m_b and a in Equation 7 (Hoek & Brown, 2019).

The parameters m_b, s and a are defined as following:

$$\sigma_1 = \sigma_3 + \sigma_{ci}\left(m_b \frac{\sigma_3}{\sigma_{ci}} + s\right)^a \tag{7}$$

$$m_b = m_i \exp\left(\frac{GSI - 100}{20 - 14D_m}\right) \tag{8}$$

$$s = \exp\left(\frac{GSI - 100}{9 - 3D_m}\right) \tag{9}$$

$$a = \frac{1}{2} + \frac{1}{6}\left(e^{-\frac{GSI}{15}} - e^{-\frac{20}{3}}\right) \tag{10}$$

The requested model parameters of the rock requested to obtain the shear criterion envelope are compressive strength of intact rocks σ_{ci}, intact rock parameter m_{br}, geological strength index GSI, and perturbation factor D_m.

Now, for the other remaining parameters, the authors considered Dm as a perturbation parameter ranging from 0 to 1, depending on the perturbation level of rock mass, and m_b as the constant for fractured mass.

The *GSI index* was determined using an empirical table proposed by Hoek (2007). *GSI* depended on the presence or not of cracks. U3 rock, which contains cracks, were
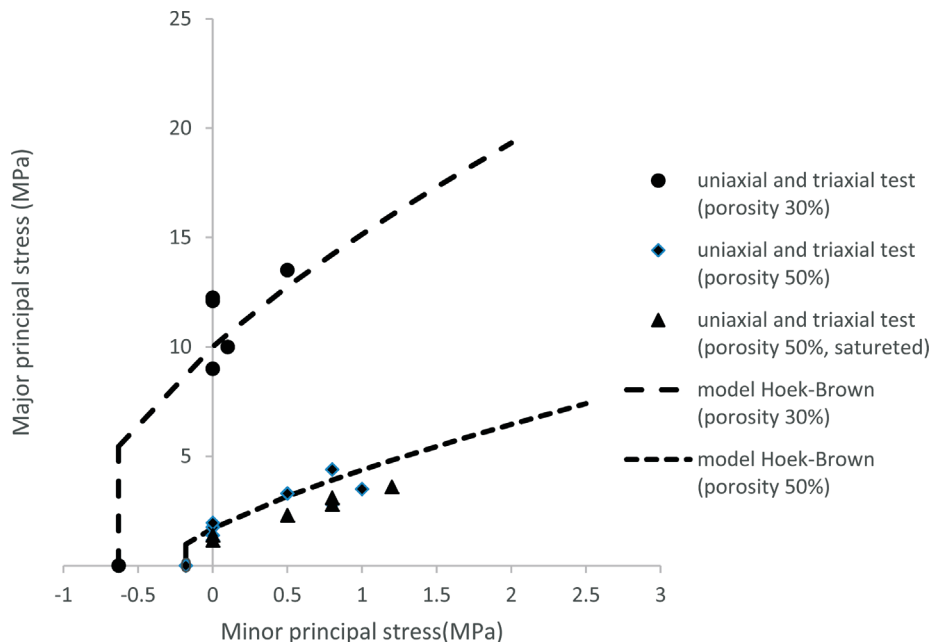
Figure 9. Hoek-Brown criterion fitted on *UCS* and triaxial tests for two different porosity (Undistributed specimens).
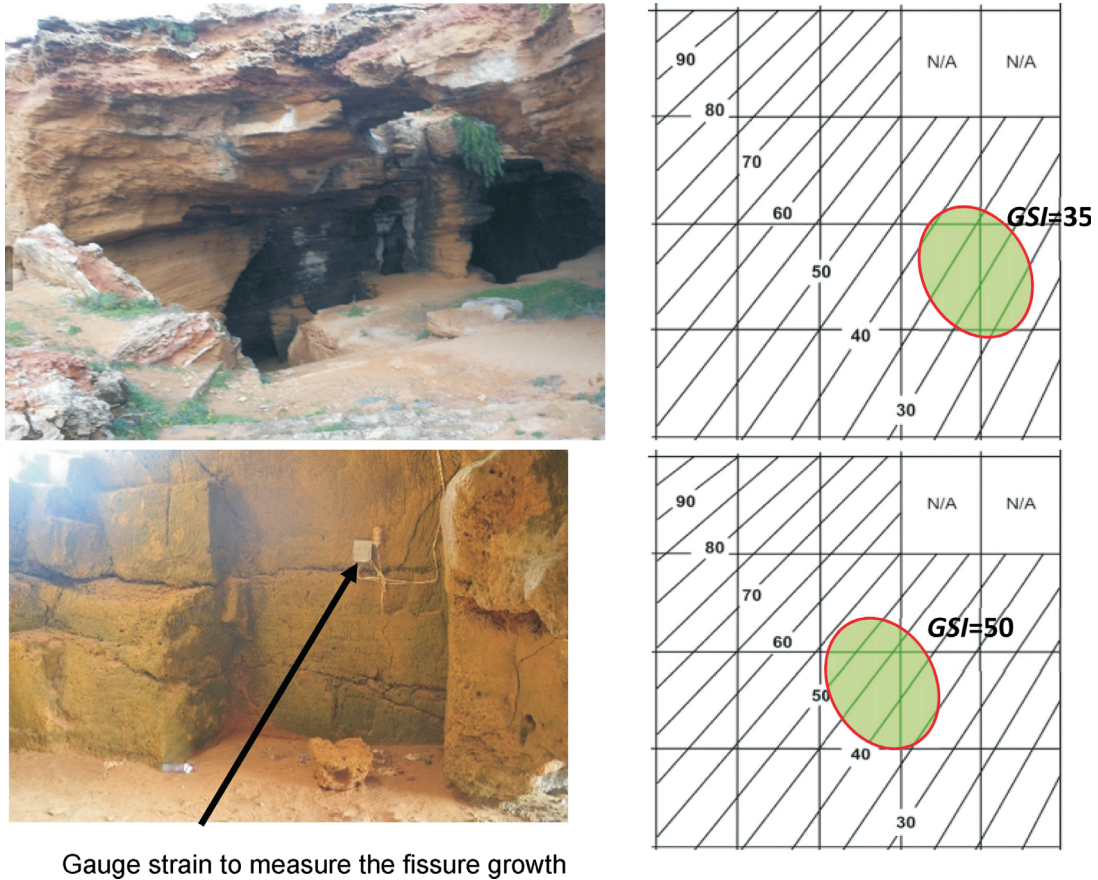
Gauge strain to measure the fissure growth

Figure 10. Horizontal and oblique fissures in U3 layer and gauge strain monitoring.

assumed to be fractured rocks. Besides, the rock mass was disturbed and its surface was strongly altered (see the photos in Figure 10). Thus, considering cracks, two *GSI* values were determined for a porosity of 50 % and of 30 %. The *Dm* value depended on the level of perturbation incurred by the mass through explosive excavation and stress relaxation. The authors used the Hoek-Brown guide to determine this disturbance factor (Hoek et al., 2002). Considering that there is no recent excavation in cave location, D_m value was set to zero. Table 3 summarizes the triaxial data and Table 4 summarizes the Hoek-Brown criterion parameters used to obtain a shear criterion for U3 rock at its

fractured state in situ (see Figure 11). In addition, to estimate the shear strength for the caves structure, rock mass deformation modulus was required. Then, using the empirical relation (Equation 9) to estimate the rock mass modulus proposed by Hoek & Diederichs (2006), U3 rock modulus was estimated considering its fractured aspect. The results are presented in Figure 12.

$$E_{rm} = E_i \left[0.02 + \frac{1 - \frac{D_m}{2}}{1 + \exp\left(\frac{60 + 15D_m - GSI}{11}\right)} \right] \quad (11)$$

Table 3. Experimental data of s_1, s_3 from triaxial test.

Porosity (%)	σ_1 (MPa)	σ_3 (MPa)
50 %	3.3	0.5
	4.4	0.8
	2.8	0.8
	3.7	1.2
35 %	13.2	0.1
	13.5	0.5

Table 4. Parameters of the generalized Hoek-Brown criterion *GSI, m_b, s, a.*

Porosity	GSI	m_b	s	a
30 %	35	1.08	0.001	0.52
50 %	35	0.294	0.001	0.52
30 %	50	1.84	0.004	0.51
50 %	50	0.53	0.004	0.51
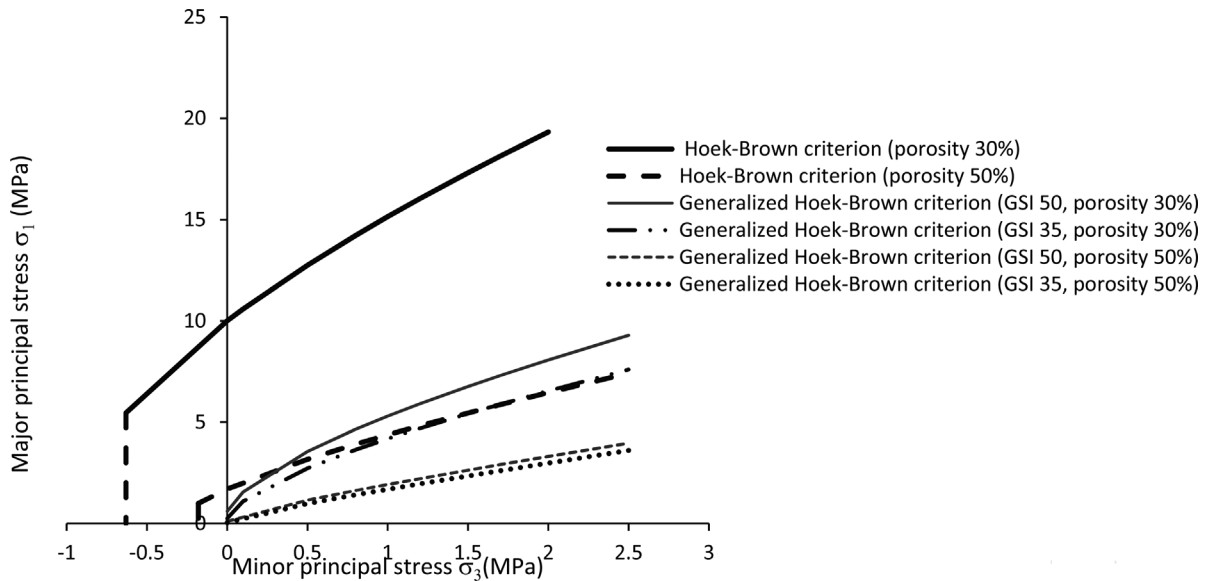
Figure 11. Generalized Hoek-Brown criterion associated to U3 rock for two porosity values.
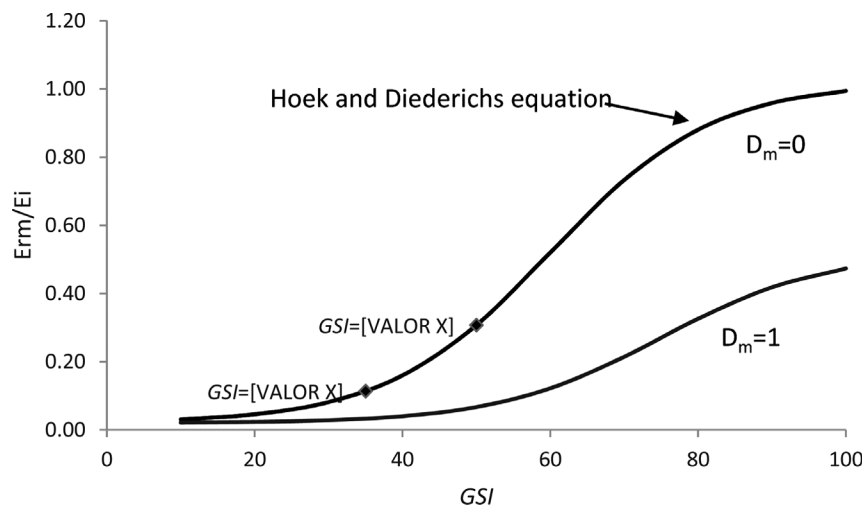
Figure 12. In-situ U3 rock mass deformation modulus for two porosity (35 % and 50 %) for two levels of perturbation ($D_m = 0$ without recent excavation, $D_m = 1$ taking into account a certain significant recent human action on the caves).

5. Conclusion

The study aimed to characterize physical and mechanical properties, compression and shear Strength, of rocks of the monument of Elhaouria caves. Therefore, physical and mineralogical characteristics along with compression and triaxial tests were conducted on sandy limestone rock samples obtained from blocks from outside of the caves structure (without any deterioration of the caves). The samples of sandy limestone rock were mainly considered as undistributed. Experimental results showed the important influence of porosity on both compression and shear strengths. Compression strength varied from 13 MPa for 33 % porosity to 1.5 MPa for 50 % porosity. Therefore, both elastic static modulus and dynamic elastic modulus,

were determined from Ultrasonic tests, depending on porosity. Their values significantly decreased with the increase of porosity. Concerning the volumetric behavior computed using measured principal strains, role of porosity was well highlighted. For example, a contractive behavior was well noted for a porosity of 50 %, for different confining stresses. Obtained results confirmed the soft rock character of U3 layer. Therefore, shear strength criterion obtained by the Generalized Hoek-Brown approach, showed low values of the compression and shear Strengths, especially for high porosity (50 % in this case). The rock mass modulus was dressed, giving a response similar to results published in Hoek & Diederichs (2006). Even though the authors tested few specimens with a larger range of porosity variation, shear Strength was clearly affected by po-

rosity. Low values of confining stress applied in triaxial experiences can be considered in the range of in-situ confining stresses (of the cave's structures), since the caves are embedded in deposit soil with a depth between 50 cm to 120 cm.

At this stage of modeling, Hoek-Brown model provided an appropriate prediction of soft rock shear criterion for sandy limestone undistributed samples, porosity variation taken into account. However, for in situ fractured rocks belonging to the caves structure, generalized Hoek-Brown model was proposed, integrating the data recently summarized in "The Hoek-Brown failure criterion and *GSI*- 2018 edition". This compression and shear criterion could be used now for any monitoring technique design. Furthermore, the associated elastoplastic model could be considered as a tool to follow the displacement field of the caves structure. Such monitoring could also help to provide efficient improvement techniques that would enhance the safety of this historic monument.

References

AFNOR NF P94-054. (1991). Roches - Détermination de la Résistance à la Compression Uniaxiale. *AFNOR - Association Française de Normalisation, Paris* (in French).

AFNOR NF P94-411. (2002). Roches - Détermination de la Vitesse de Propagation des Ondes Ultrasonores en Laboratoire - Méthode par Transparence. *AFNOR - Association Française de Normalisation, Paris* (in French).

AFNOR NF P94-420. (2000). Sols: Reconnaissance et Essais - Détermination de la Masse Volumique des Particules Solides des Sols - Méthode du Pycnomètre à Eau. *AFNOR - Association Française de Normalisation, Paris* (in French).

ASTM D7012-04. (2004). Standard Test Method for Compressive Strength and Elastic Moduli of Intact Rock Core Specimens under Varying States of Stress and Temperatures. *ASTM International, West Conshohocken, PA*. https://doi.org/10.1520/D7012-04

Al-Omari, A., Beck, K., Brunetaud, X., Török, Á., & Al-Mukhtar, M. (2015). Critical degree of saturation: A control factor of freeze-thaw damage of porous limestones at Castle of Chambord, France. *Engineering Geology*, 185, 71-80.

http://dx.doi.org/10.1016/j.enggeo.2014.11.018

Aldoasri M.A., Darwish S.S., Adam M.A., Elmarzugi N.A., & Ahmed, S.M. (2017). Enhancing the durability of calcareous stone monuments of ancient Egypt using $CaCO_3$ nanoparticles. *Sustainability*, 9(8), 1392. https://doi.org/10.3390/su9081392

Asef, M.R., & Farrokhrouz, M. (2010). Governing parameters for approximation of carbonates. *Electronic Journal of Geotechnical Engineering*, 15, 1581-1592.

Baud, P., lle Kleina, E., & Wongb, T.F. (2004). Compaction localization in porous sandstones: Spatial evolution of damage and acoustic emission activity. *Journal of Structural Geology*, 26(4), 603-624. http://dx.doi.org/10.1016/j.jsg.2003.09.002

Baud, P., Wong, T.F., & Zhu, W. (2014). Effects of porosity and crack density on the compressive strength of rocks. *International Journal of Rock Mechanics and Mining Sciences*, 67, (April 2014), 202-211. http://dxdoiorg /101016/jijrmms201308031

Bosio, J.J., & Kanji, M.A. (1998). Soft rocks of the Rio de la Plata Basin. *Proc. 2nd International Symposium on Indurated Soils and Soft Rocks*, *Naples*. Balkema, 65-71.

Daoud, H.S., Rashed, K.A., & Alshkane, Y.M. (2017). Correlations of uniaxial compressive strength and modulus of elasticity with point load strength index, pulse velocity and dry density of limestone and sandstone rocks in Sulaimani Governorate, Kurdistan Region, Iraq. *Journal Zankoy Sulaimani Part A (Pure Appl. Sci.)*, 19(3-4), 57-72. https://doi.org/10.1002/2017JB014627

Elliot, G.M., & Brown, E.T. (1985). Yield of a soft, high porosity rock. *Géotechnique*, 35(4), 413-423. https://doi.org/10.1680/geot.1985.35.4.413

Evans, B., Fredrich, J.T., & Wong, T-F. (1990). The brittle-ductile transition in rocks: Recent theoretical and experimental progress. *Geophysical Monograph Series*, 56, 1-20, https://doi.org/10.1029/GM056p0001

Guilloux, A. (2005). Note sur la définition des "sols indurés roches tendres" (SIRT). *Revue Française de Géotechnique*, 111, 59-66 (in French). https://doi.org/10.1051/geotech/2005111059

ISO 5017:2013. (2013). Dense Shaped Refractory Products - Determination of Bulk Density, Apparent Porosity and True Porosity. *ISO - International Organization for Standardization, Geneva*. https://www.iso.org/standard/56179.html

Kanji, M.A. (2014). Critical issues in soft rocks. *Journal of Rock Mechanics and Geotechnical Engineering*, 6(3), 186-195. https://doi.org/10.1016/j.jrmge.2014.04.002

Koubaa, Y., Jamei M., & Guiras H. (2018). Hydro-mechanical properties of highly porous limestone rock used for historic monuments in North-East Tunisia. *Journal of Civil and Environmental Engineering*, 8(3), 1000310. https://doi.org/10.4172/2165-784X.1000310

Harrazi, N. (1995). *Les Carrières Antiques d'el Haouaria: The Ancient Quarries of el Haouaria*. Agence nationale du Patrimoine, Tunis.

Hoek, E., Carranza-Torres, C., & Corkum, B. (2002). Hoek-Brown criterion - 2002 edition. *Proc. 5th North American Rock Mechanics Symposium & 17th Tunnelling Association of Canada Conference, Toronto*. Vol. 1, University of Toronto, 267-273.

Hoek, E., & Diederichs, M.S. (2006). Empirical estimation of rock mass modulus. *International Journal of Rock Mechanics and Mining Sciences*, 43(2), 203-215. http://doi.org/10.1016 /j.ijrmms.2005.06.005

Hoek, E. (2007). *Practical Rock Engineering. E-book version.* Rocscience Editors.

Hoek, E., & Brown, E.T. (2019). The Hoek-Brown failure criterion and GSI-2018 edition. *Journal of Rock Mechanics ang Geotechnical Engineering*, 11(3), 445-463. https://doi.org/10.1016/j.jrmge.2018.08.001

Nicolas, A., Fortin, J., Regnet, J.B., Dimanov, A., & Gueguen, Y. (2016). Brittle and semibrittle behaviours of a carbonate rock: influence of water and temperature. *Geophysical Journal International*, 206(1), 438-456. https://doi.org/10.1093/gji/ggw154

Price, A.M., & Farmer, I.W. (1979). Application of yield models to rock. *International Journal of Rock Mechanics and Mining Sciences & Geomechanics Abstracts*, 16(2), 157-159. https://doi.org/10.1016/0148-9062(79)91454-2

Rahmouni, A., Boulanouar, A., Samaouali, A., Boukalouch, M., Géraud, Y., & Sebbani, J. (2017). Prediction of elastic and acoustic behaviors of calcarenite used for construction of historical monuments of Rabat, Morocco. *Journal of Rock Mechanics and Geotechnical Engineering*, 9(1), 74-83. https://doi.org/10.1016/j.jrmge.2016.11.005

Paskoff, R., & Sanlaville, P. (1983). *Les Côtes de la Tunisie. Variations du Niveau Marin Depuis le Tyrrhénien.* Collection de la Maison de l'Orient et de la Méditerranée Jean Pouilloux, 14(1). ERA 345 du CNRS (in French).

Romero, E. (1999). *Characterization and thermo-hydromechanical behavior of unsaturated boom clay* [Doctoral thesis, Polytechnic University of Catalonia]. Polytechnic University of Catalonia's repository. http://hdl.handle.net/2117/93536

Yu, S., & Oguchi, C.T. (2010). Role of pore size distribution in salt uptake, damage, and predicting salt susceptibility of eight types of Japanese building stones. *Engineering Geology*, 3(115), 226-236. http://dx.doi.org/10.1016/j.enggeo.2009.05.007

Zuo, J.P., Li, H.T., Xie, H.P., Ju, Y., & Peng, S.P. (2008). A nonlinear strength criterion for rock like materials based on fracture mechanics. *International Journal of Rock Mechanics and Mining Sciences*, 45(4), 594-599. https://doi.org/10.1016/j.ijrmms.2007.05.010

Zuo, J.P., Liu, H., & Li, H. (2015). A theoretical derivation of the Hoek-Brown failure criterion for rock materials. *Journal of Rock Mechanics and Geotechnical Engineering*, 7(4), 361-366. https://doi.org/10.1016/j.jrmge.2015.03.008